Click Here for Full Article

# EMAG2: A 2−arc min resolution Earth Magnetic Anomaly Grid compiled from satellite, airborne, and marine magnetic measurements

**S. Maus**

*CIRES, University of Colorado at Boulder, Boulder, Colorado 80309, USA*

*National Geophysical Data Center, NOAA, E/GC1, 325 Broadway, Boulder, Colorado 80305-3328, USA (stefan.maus@noaa.gov)*

**U. Barckhausen**

*Federal Institute for Geosciences and Natural Resources, D-30655 Hannover, Germany*

**H. Berkenbosch**

*GNS Science, 1 Fairway Drive, Avalon, P.O. Box 30 368, Lower Hutt, New Zealand*

**N. Bournas**

*Geotech Ltd., Aurora, Ontario L4G 4C4, Canada*

**J. Brozena**

*Marine Physics Branch, Naval Research Laboratory, Code 7420, 4555 Overlook Avenue SW, Washington, D. C. 20375, USA*

**V. Childers**

*National Geodetic Survey, NOAA, 1315 East-West Highway, SSMC-3, Silver Spring, Maryland 20910, USA*

**F. Dostaler**

*Geological Survey of Canada, 615 Booth Street, Ottawa, Ontario K1A 0E9, Canada*

**J. D. Fairhead**

*GETECH, Kitson House, Elmete Hall, Elmete Lane, Leeds LS8 2LJ, UK*

*School of Earth and Environment, University of Leeds, Earth Science Building, Leeds LS2 9JT, UK*

**C. Finn**

*U.S. Geological Survey, Denver Federal Center, P.O. Box 25046, MS 964, Denver, Colorado 80225, USA*

**R. R. B. von Frese**

*School of Earth Sciences, Ohio State University, Columbus, Ohio 43210, USA*

**C. Gaina**

*Geological Survey of Norway, Leiv Eirikssonsvei 39, Trondheim N-7491, Norway*

**S. Golynsky**

*All-Russian Research Institute for Geology and Mineral Resources of the World Ocean, 1 Angliysky Avenue, Saint Petersburg 190121, Russia*

**R. Kucks**

*U.S. Geological Survey, Denver Federal Center, P.O. Box 25046, MS 964, Denver, Colorado 80225, USA*

**H. Lühr**

*Helmholtz Centre Potsdam, German Research Centre for Geosciences, D–14473 Potsdam, Germany*

**P. Milligan**

*Geoscience Australia, Canberra, ACT 2601, Australia*

**S. Mogren**

*College of Sciences, King Saud University, Riyadh 11451, Saudi Arabia*

**R. D. Müller**

*School of Geosciences, University of Sydney, Sydney, New South Wales 2006, Australia*

**O. Olesen**

*Geological Survey of Norway, Leiv Eirikssonsvei 39, Trondheim N–7491, Norway*

**M. Pilkington**

*Geological Survey of Canada, 615 Booth Street, Ottawa, Ontario K1A 0E9, Canada*

**R. Saltus**

*U.S. Geological Survey, Denver Federal Center, P.O. Box 25046, MS 964, Denver, Colorado 80225, USA*

**B. Schreckenberger**

*Federal Institute for Geosciences and Natural Resources, D–30655 Hannover, Germany*

**E. Thébault**

*Institut de Physique du Globe de Paris, 4 place Jussieu, F–75252 Paris, France*

**F. Caratori Tontini**

*Istituto Nazionale di Geofisica e Vulcanologia, via Pezzino Basso, 2, I–19020 Fezzano, Italy*

[1] A global Earth Magnetic Anomaly Grid (EMAG2) has been compiled from satellite, ship, and airborne magnetic measurements. EMAG2 is a significant update of our previous candidate grid for the World Digital Magnetic Anomaly Map. The resolution has been improved from 3 arc min to 2 arc min, and the altitude has been reduced from 5 km to 4 km above the geoid. Additional grid and track line data have been included, both over land and the oceans. Wherever available, the original shipborne and airborne data were used instead of precompiled oceanic magnetic grids. Interpolation between sparse track lines in the oceans was improved by directional gridding and extrapolation, based on an oceanic crustal age model. The longest wavelengths (>330 km) were replaced with the latest CHAMP satellite magnetic field model MF6. EMAG2 is available at http://geomag.org/models/EMAG2 and for permanent archive at http://earthref.org/cgi-bin/er.cgi?s=erda.cgi?n=970.

# 1. Introduction

[2] Magnetic anomaly maps provide insight into the subsurface structure and composition of the Earth's crust [*Vine and Matthews*, 1963; *Vine*, 1966; *Langel and Hinze*, 1998; *Golynsky*, 2002; *Purucker and Whaler*, 2007]. Over continental areas, magnetic anomalies illuminate geologic, tectonic, and geothermal evolution of crust and lithosphere [*Shaw et al.*, 1996; *Milligan et al.*, 2003; *Hemant and Maus*, 2005; *Whittaker et al.*, 2007; *Aitken and Betts*, 2008]. In the world's oceans, anomalies trending parallel to the isochrons (lines of equal age) reveal the temporal evolution of oceanic crust [*Müller et al.*, 2008]. Magnetic maps are widely used in the geological sciences [*Hinze*, 1985] and in resource exploration [*Gibson and Millegan*, 1998; *Hildenbrand et al.*, 2000]. Furthermore, the global magnetic map is useful in detailed studies [*Blaich et al.*, 2009] and science education to illustrate various aspects of Earth evolution such as plate tectonics and crustal interaction with the deep mantle. Distinct patterns and magnetic signatures can be attributed to the formation (seafloor spreading) and destruction (subduction zones) of oceanic crust [*Nakanishi et al.*, 1992], the formation of continental crust by accretion of various terranes to cratonic areas [*Roest et al.*, 1995; *Bokelmann and Wüstefeld*, 2009] and large-scale volcanism, both on continents and oceans [*Bradley*, 1988; *Saltus and Hudson*, 2007].

[3] Our first global magnetic anomaly grid, the National Geophysical Data Center's candidate grid for the World Digital Magnetic Anomaly Map [*Maus et al.*, 2007b] is enjoying widespread use. It was incorporated into Google Earth (http://bbs.keyhole.com/ubb/ubbthreads.php?ubb=showflat&Number=922040&site_id=1) and NASA World Wind (http://www.getech.com/downloads/WDMAM.htm) and was selected as the base grid for the official World Digital Magnetic Anomaly Map [*Korhonen et al.*, 2007] of the Commission of the World Geological Map (CWGM, http://ccgm.free.fr/). A significant shortcoming of this first grid was the sparse coverage in the southern oceans.

[4] To improve the visual appearance of the CWGM print edition, unsurveyed areas in the oceans were filled with synthetic magnetic anomalies. Here we provide an alternative approach which avoids the use of synthetic data. The field is extrapolated into unsurveyed areas using directional gridding, based on the oceanic crustal age model by *Müller et al.* [2008]. To further improve the representation of magnetic anomalies over the oceans, we avoided precompiled oceanic anomaly grids and reverted to the original track line data where available. All data with time stamp and original magnetic measurement were reprocessed by subtracting the Comprehensive Model CM4 [*Sabaka et al.*, 2004] which provides a better main field representation than the International Geomagnetic Reference Field (IGRF [*Maus et al.*, 2005]) and further includes corrections for external magnetic fields. Line leveling was used to minimize crossover errors. The resulting improvements are particularly visible off the coasts of North America, Australia and Antarctica. The original oceanic data were not used in the Arctic, for which a new grid has just been released (C. Gaina, S. Werner, and Group CAMP-GM, Circum-Arctic Mapping Project: New magnetic and gravity anomaly maps of the Arctic, paper presented at 33rd International Geological Congress, StatoilHydro, Oslo, Norway, 2008), and East Asia, where the grid of the Coordinating Committee for Geoscience Programmes in East and Southeast Asia (http://www.ccop.or.th/) was used. Finally, the long-wavelength anomaly field (wavelengths >330 km), given by the latest CHAMP lithospheric field model MF6 [*Maus et al.*, 2008], was substituted into the grid.

# 2. Processing Sequence

[5] The processing sequence for EMAG2 had the following steps: (1) merging of existing grids at 4 km altitude above the geoid using least squares collocation, (2) processing of ship and airborne measurements, (3) line leveling of the track line data, (4) merging of track line data with the grid at 4 km altitude using least squares collocation with anisotropic correlation function over the oceans, and (5) substitution of spherical harmonic degrees $\leq 120$ ($\geq 330$ km wavelength) with the CHAMP satellite magnetic anomaly model MF6 [*Maus et al.*, 2008]. Some of these steps have been described in detail by *Maus et al.* [2007b] and will therefore only briefly be recounted here.

## 2.1. Merging of Precompiled Grids

[6] Over land, preexisting country-wide continental-scale grids derived from airborne surveys were merged by least squares collocation into a common global grid, following the procedure described by *Maus et al.* [2007b, section 4.1]. A resolution of 1 arc min at a height of 4 km above the geoid was chosen for the common grid. The oceanic grids of the Arctic and of East Asia were also included in this proce-
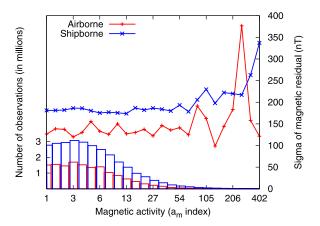
**Figure 1.** Root mean square residuals were computed for all individual tracks. They were then averaged in bins of equal magnetic activity and plotted against the $a_m$ magnetic activity index. Shown also is the histogram of observations. Only very few observations at the highest magnetic activity levels appear to be significantly affected by external magnetic disturbances.

dure. For all other ocean areas we used the original track line data, as described below.

## 2.2. Processing of Ship and Airborne Measurements

[7] Measurements over oceans came primarily from three sources: Ship track data contributed by numerous institutions to NGDC's GEODAS marine data archive, marine and aeromagnetic data released with the 2001 map edition of the Antarctic Digital Magnetic Anomaly Project [*Golynsky et al.*, 2001], and the Project Magnet airborne data of the Naval Research Lab (NRL). All data providers are listed in the acknowledgements of this paper.

[8] For NGDC's previous candidate grid for World Digital Magnetic Anomaly Map (WDMAM), we used marine track line magnetic residuals given in the GEODAS marine track line data archive. These residuals were calculated by subtracting global reference models (e.g., the International Geomagnetic Reference Field [*Maus et al.*, 2005]) from total field observations and are known to have large offsets [*Chandler and Wessel*, 2008]. One of the main sources of these offsets is the poor quality of the reference models. In the processing of data for our candidate grid for WDMAM, we argued that the offsets were largely removed in subsequent line leveling, but in fact a better result is obtained if a higher-quality reference model is removed prior to line leveling. The line leveling is then started with a cleaner initial data set. For EMAG2 we therefore reverted to the original measurements (if these were

not available then we continued to use the provided residuals) and subtracted the CM4 model [*Sabaka et al.*, 2004] which provides the best available representation of the main, ionospheric and magnetospheric fields. The correction using CM4 reduced root mean square (RMS) crossover errors from about 400 nT to 92 nT. For the previous WDMAM processing, we had used NRL Project Magnet data from which CM4 had been subtracted by D. Ravat (personal communication, 2005). For EMAG2, all NRL data were reprocessed for consistency with the marine data.

[9] For satellite observations of the Earth's crustal magnetic field, disturbances by external fields are a serious issue. Satellite magnetic measurements are significantly affected by external field contamination at lowest activity levels. To test the effect of external field disturbances on near-Earth observations we therefore plotted the RMS of the residuals, after subtracting CM4 from the aeromagnetic and marine track line data, against magnetic activity. As a measure of magnetic activity, we used the $a_m$ index [*Menville and Paris*, 2007], which is quite similar to the more widely known Kp index. The $a_m$ index is available from the International Service of Geomagnetic Indices (http://isgi.cetp.ipsl.fr). The ISGI Web site also provides background information on the production of this index. As shown in Figure 1, marine and aeromagnetic residuals are not greatly affected by the level of geomagnetic disturbance, most likely because the proximity of the ship and airborne measurements to the crustal sources results in a much better signal to noise ratio than for satellite measurements. A visible deterioration only sets in at $a_m > 100$ (approximately Kp > 7), which we therefore used as a threshold for the rejection of individual measurements for both marine and aeromagnetic measurements. We further discarded entire track segments, for which the standard deviation of the magnetic residuals exceeded 1000 nT. Finally, we discarded segments in which the standard deviation of the magnetic residual gradient exceeded 100 nT/km for shipborne and 50 nT/km for airborne data. Here, a track segment is defined as a continuous sequence of measurements with approximately constant direction.

## 2.3. Line Leveling

[10] All track line data were line-leveled using the algorithm described by *Maus et al.* [2007b, section 2.2]. However, we significantly reduced the search radius from the previously used $R_s = 100$ km to $R_s = 8$ km in order to concentrate on minimizing cross-
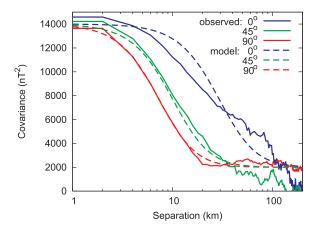
**Figure 2.** Observed oceanic correlation functions estimated from the line-leveled shipborne data for different directions relative to the local isochron as given by the oceanic crustal age model by *Müller et al.* [2008]. Overlain are the model correlation functions $V_3$ [*Maus et al.*, 2007b] for $V_0 = 12{,}000$ nT$^2$ with an additional along-track correlated variance of 2000 nT$^2$, shown for $R_c(0°) = 28$ km, $R_c(45°) = 9.6$ km, and $R_c(90°) = 7$ km.

over offsets. Furthermore, we allowed for slightly shorter-wavelength adjustments, reflecting the higher resolution of the MF6 over the previously used MF5 model [*Maus et al.*, 2007a]. While the number of correction coefficients per track was previously determined by $N_i = trunc(D_i/400$ km$) + 1$, we now used $N_i = trunc(D_i/300$ km$) + 1$. Line leveling reduced crossover errors from 92 nT to 70 nT and reduced the misfit to the merged grid from 121 nT to 97 nT RMS.

## 2.4. Anisotropic Least Squares Collocation

[11] Least squares collocation (LSC) provides a magnetic field estimate for a desired location (e.g., a grid cell center) from all surrounding measurements, based on a covariance model of the magnetic field [*Maus et al.*, 2007b, section 2.1]. The first step in LSC is to estimate the correlation function. For land areas we used the observed correlation function of the previous study [*Maus et al.*, 2007b, Figure 1]. However, we noticed that the previously assumed flight altitude of 1000 m was unrealistically high, particularly for Australia where most of the surveys were flown with 100 m terrain clearance [*Milligan and Franklin*, 2004]. For a given observed correlation function, the lower the assumed survey altitude, the lower the estimated variance $V_0$ and the shorter the estimated correlation length $R_c$. We therefore reduced the value for the assumed variance $V_0$ from previously 40,000 nT$^2$ to now 33,000 nT$^2$ and the

correlation length $R_c$ from 15 km to 14 km for land areas in order to better represent the true survey parameters.

[12] Using the line-leveled marine magnetic data, we then carried out a similar correlation analysis for the oceans, taking the anisotropy of ocean magnetic anomalies into account. The track line data were divided into track segments with constant heading direction. To avoid the effect of arbitrary offsets between the measurements on different tracks, only pairs of values belonging to the same track were used in estimating the correlation function. For every pair, the azimuth of the connecting line was computed and compared with the direction of the isochrons at the locations of both points. The pair was discarded if the azimuth of the isochrons was not well defined at one of the points, the azimuth differed by more than 5° between the points, or the topographic gradient between the two points exceeded 3%. The latter exclusion was introduced to avoid contamination by magnetic anomalies due to sea mounts. The anisotropic correlation function was then computed in 10° directional bins, where 0° represents the direction parallel to the isochrons and 90° is in the spreading direction.

[13] Figure 2 shows that the observed correlation functions are consistent with the $V_3$ correlation function model with $R_c(0°) = 28$ km in isochron direction and $R_c(90°) = 7$ km in spreading direction, $V_0 = 12{,}000$ nT$^2$ and with an additional along-track correlated variance of 2000 nT$^2$ appearing here as an upward shift of the model. Assuming that $R_c$ has an elliptical directional dependence leads to $R_c(45°) = 9.6$ km which is consistent with the observed correlation for this angle. This ellipse is consistent with the circle $R_c = 14$ km used for land areas, stretched by a factor 2 in the isochron direction and compressed by a factor 2 in the spreading direction. This anisotropic correlation model allows us to use LSC as a directional gridding algorithm.

[14] While this covariance model fits the observed data very well, using it "as is" in the collocation leads to a problem: The covariance falls off too rapidly, even in the isochron direction. When extrapolating the field far out from a track line, the estimate quickly decays to zero, producing white stripes parallel to the track lines. We therefore increased the correlation length by a factor 2 in the gridding of the ocean areas. This significantly improves the visual appearance of the resulting map. We include a "health warning" indicating that over the oceans the map is smoother than the true magnetic field. However, the factor 4 anisotropy of
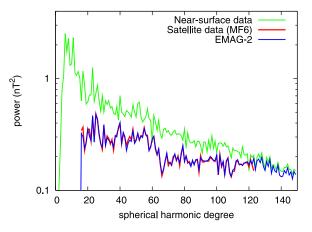
**Figure 3.** The original spectrum of the merged ship-borne and airborne magnetic anomaly grid is shown in green. Substitution with the satellite-derived magnetic field model MF6 (red) leads to the final EMAG2 grid, its spectrum shown in blue. All spectra are shown in the normalization of *Maus* [2008].

the true correlation function was maintained. The anisotropy of the oceanic field displayed in the map is therefore realistic, even if the overall appearance is smoother than real over the oceans.

[15] A further concern is that inaccuracies in the oceanic crustal age model [*Müller et al.*, 2008] and resulting errors in the isochron direction could lead to the distortion of oceanic magnetic anomalies. As indicated in the error estimates provided with the oceanic age model [*Müller et al.*, 2008], the absence of reversals during the Cretaceous normal super-chron (about 120 Ma to 83 Ma) is not seen as a major source of uncertainty in the isochron direction. For even older oceanic crustal ages, however, reversal patterns in oceanic magnetic anomalies tend to be more difficult to identify. Because of the limited spatial extent of older crust, a quantitative estimate of its magnetic anisotropy was difficult to obtain for this study, and we therefore found the appropriate factors by trial and error. A realistic appearance of linear anomalies in the western Pacific ocean was obtained by maintaining the factor 4 anisotropy up to an age of 140 Ma and tapering off to a lower factor of 2.25 for oceanic crust older than 150 Ma. This reduction in anisotropy also addresses concerns with the accuracy of the oceanic crustal age model at older crustal ages. While the oceanic age model is reliable for younger crust, the authors indicate
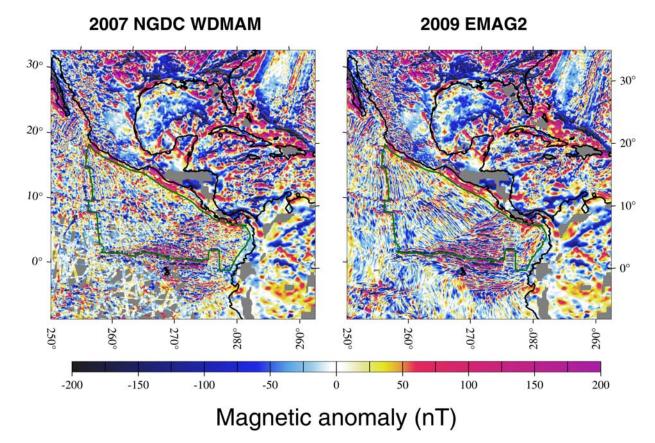


**Figure 4.** Comparison of NGDC's candidate grid for WDMAM and EMAG2. The boundaries of the Cocos plate off the west coast of Central America are shown in green. Reprocessing of the original track line data and directional gridding significantly improved the representation of oceanic magnetic lineations.
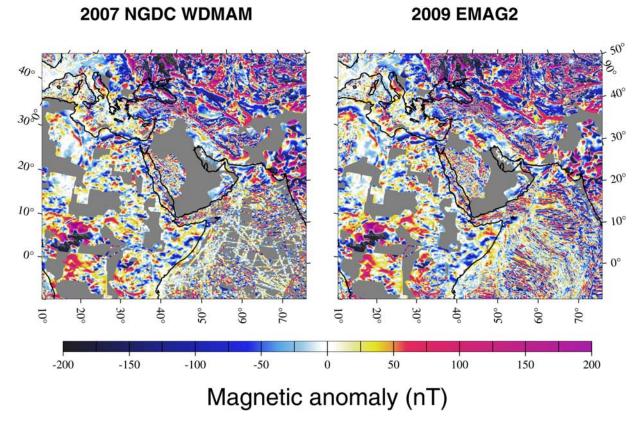
**2007 NGDC WDMAM**    **2009 EMAG2**

Magnetic anomaly (nT)

**Figure 5.** Comparison of NGDC's candidate for WDMAM and EMAG2 for northern Africa, Mediterranean, and the Middle East.

higher uncertainties over older crust. Possible distortions of magnetic anomalies over older crust were thus reduced by employing a lower anisotropy factor in gridding the field over those regions.

## 2.5. Long-Wavelength Substitution With Satellite Model

[16] Long-wavelength magnetic anomalies are not reliably represented in the merged grid of ship and airborne data. This is primarily due to adjustments made in stitching together a large number of individual surveys with typical dimensions of tens to hundreds of kilometers. It is therefore essential to correct the long-wavelength field by substituting the longest wavelengths with a magnetic field model derived from satellite magnetic measurements.

[17] From the merged grid at 4 km altitude above the geoid we first estimated the coefficients of a spherical harmonic expansion of the magnetic potential up to degree 150. By using the least squares method and eliminating the lowest eigenvalues, we selected the magnetic potential with the least power that represented the observed anomaly. For every grid point, we then computed the total field anomaly

for this model to degree 120, subtracted it from the grid value and finally added the magnetic anomaly given by the MF6 magnetic field model [*Maus et al.*, 2008] to degree 120. For validation we then estimated the spectrum of the final grid [*Maus*, 2008]. The three spectra are shown in Figure 3. The slight discrepancy between the blue and green curves at degrees >120 should not be interpreted as a true difference in the spectral content of the original and long-wavelength-corrected grids. The difference is due to the leakage of long-wavelength power to short wavelengths in the spectral estimation.

## 3. Discussion of Result

[18] In this section we compare the final EMAG2 grid with our previous candidate grid for WDMAM [*Maus et al.*, 2007b] for three selected regions in Figures 4–6. Finally, Figure 7 displays a global map of EMAG2. Note that EMAG2 represents magnetic anomalies at 4 km altitude above the geoid in 2–arc min resolution, while the WDMAM grid was specified at 5 km altitude in 3–arc min resolution.

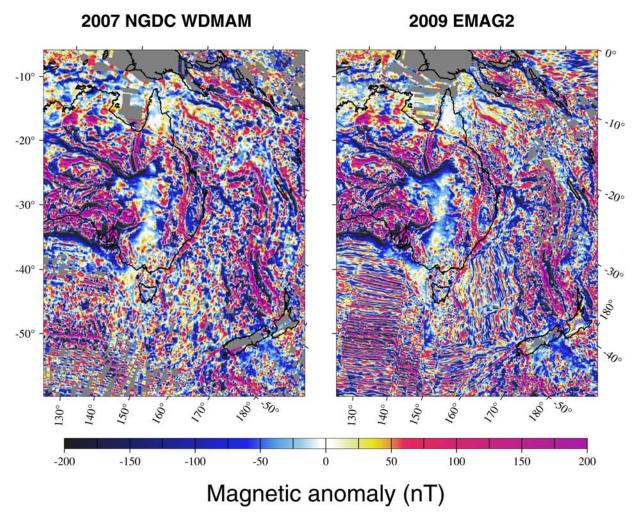[19] Figure 4 shows the Cocos plate off the west coast of Central America. This plate has strong

**Figure 6.** Comparison of NGDC's candidate for WDMAM and EMAG2 for eastern Australia and New Zealand. Better data coverage and directional gridding significantly improved the representation of magnetic anomalies in this region.

magnetic anomalies, oriented both north-south and east-west. Directional gridding by LSC using an anisotropic correlation function enables us to fill in unsurveyed areas leading to a better representation of the magnetic lineations. Figure 4 illustrates another deficiency of the previous WDMAM map, which included oceanic coverage of the North American Magnetic Anomaly Grid (NAMAG). While the latter grid has a high resolution of 1 km, marine magnetic anomalies are not represented in full detail. Reverting to the original marine track line data enabled us to better represent the shorter-wavelength magnetic lineations over the oceans in EMAG2, as seen in the northern half of the Cocos plate.
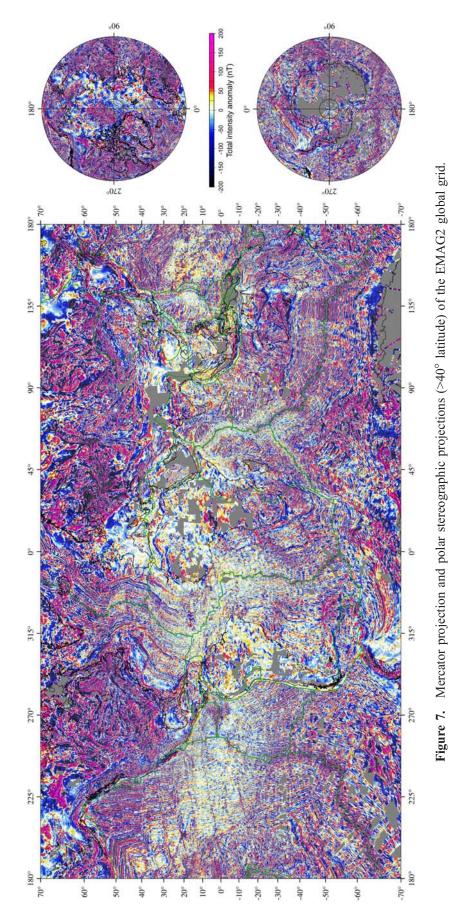
[20] Coverage of northern Africa, the Mediterranean and the Middle East (Figure 5) has been improved by including additional aeromagnetic surveys of Algeria, Saudi Arabia, Iraq, Pakistan and Afghanistan. Italy and its surrounding seas were updated by digitizing the published map of *Tontini et al.* [2004].

[21] From 2007 to 2008, large contributions of marine magnetic data have been made to the NGDC GEODAS archive by Australia [*Milligan and Franklin*, 2004] and New Zealand. These have had a significant impact on defining the oceanic magnetic anomalies in the surrounding seas and Indian Ocean, as illustrated in Figure 6. Three aeromagnetic surveys of New Zealand were also newly included.

[22] A global map of EMAG2 is displayed in Figure 7. A similar map in poster format with

**Figure 7.** Mercator projection and polar stereographic projections (>40° latitude) of the EMAG2 global grid.

additional explanations and acknowledgements can be downloaded from http://geomag.org/models/EMAG2.

## 4. Conclusions and EMAG2 Availability

[23] EMAG2 presents a significant improvement over NGDC's WDMAM candidate grid. The resolution has been improved from 3 arc min (about 5.5 km) to 2 arc min (about 3.7 km). Correspondingly, the altitude has been decreased from 5 km to 4 km above geoid. Additional grids and track line data sets have been incorporated in order to improve the data coverage over land and ocean areas. The use of an anisotropic correlation model has led to a more realistic representation of oceanic magnetic lineations and has improved the interpolation and extrapolation of the grid in sparsely surveyed regions, particularly in the southern oceans. On a cautionary note, however, oceanic isochrons must be inferred from the original marine and aeromagnetic profiles, rather than from EMAG2. Remaining "gray" patches indicate the continuing need for marine and aeromagnetic data collection efforts to fill in unsurveyed areas.

[24] Detailed regional studies show that the Earth's crustal composition and its geodynamic evolution are directly reflected in its geophysical properties. Global magnetic anomaly maps can be used to investigate patterns that characterize individual geodynamic domains (for example linear stripes for the oceanic areas versus bulky pattern for continents), identify large zones of volcanic provinces (high magnetic amplitudes) both onshore and offshore and to identify and analyze regional features reflected in long-wavelength magnetic anomalies (for example suture zones that show the location of collisions, Large Igneous Provinces, cratonic areas).

[25] The extensive coverage, consistency and high resolution of EMAG2 opens a number of important new opportunities, such as (1) global comparisons and testing of geologic structural/tectonic hypotheses and models, (2) investigation of tectonic/structural relationships that cross land/ocean boundaries, (3) development and validation of continental plate reconstructions, (4) synrift exploration of the continental margins [Somerton et al., 2009], (5) extension of quantitative magnetic interpretation methods [Blakely, 1995] to regional and global scales, (6) placing local interpretations/models into the regional and global context, and (7) global mapping of the depth to the Curie isotherm. Furthermore, EMAG2 will constitute the data basis for the upcoming revision of the NGDC-720 model (http://www.ngdc.noaa.gov/geomag/EMM/emm.shtml). Using a spherical harmonic representation of the magnetic potential to degree and order 720 [Maus, 2008], the NGDC-720 model provides the vector of the magnetic field at a resolution of about 15 arc min.

[26] The EMAG2 grid is permanently archived at http://earthref.org/cgi-bin/er.cgi?s=erda.cgi?n=970. It is also available for download from http://geomag.org/models/EMAG2, together with supplemental materials such as a poster version and plug-ins for Google Earth and Google Maps, the latter also being accessible at http://bbs.keyhole.com/ubb/ubbthreads.php?ubb=showflat&Number=1205597. A package for visualization in NASA World Wind can be downloaded from http://www.getech.com/downloads/EMAG2.htm.

## Acknowledgments

# References

Aitken, A. R. A., and P. G. Betts (2008), High-resolution aeromagnetic data over central Australia assist Grenville-era (1300–1100 Ma) Rodinia reconstructions, *Geophys. Res. Lett.*, *35*, L01306, doi:10.1029/2007GL031563.

Blaich, O. A., J. I. Faleide, F. Tsikalas, D. Franke, and E. Leon (2009), Crustal-scale architecture and segmentation of the Argentine margin and its conjugate off South Africa, *Geophys. J. Int.*, *178*, 85–105, doi:10.1111/j.1365-246X.2009.04171.x.

Blakely, R. J. (1995), *Potential Theory in Gravity and Magnetic Applications*, Cambridge Univ. Press, Cambridge, U. K.

Bokelmann, G. H. R., and A. Wüstefeld (2009), Comparing crustal and mantle fabric from the North American craton using magnetics and seismic anisotropy, *Earth Planet. Sci. Lett.*, *277*, 355–364.

Bradley, L. (1988), Constraints on the crustal nature and tectonic history of the Kerguelen Plateau from comparative magnetic modeling using MAGSAT data, *Tectonophysics*, *145*, 243–251, doi:10.1016/0040-1951(88)90198-9.

Chandler, M. T., and P. Wessel (2008), Improving the quality of marine geophysical track line data: Along-track analysis, *J. Geophys. Res.*, *113*, B02102, doi:10.1029/2007JB005051.

Gibson, R. I., and P. S. Millegan (1998), *Geologic Applications of Gravity and Magnetics: Case Histories*, *AAPG Stud. in Geol.*, vol. 43, Soc. of Explor. Geophys., Tulsa, Okla.

Golynsky, A. (2002), The composite magnetic anomaly map of East Antarctic, *Tectonophysics*, *347*, 109–120, doi:10.1016/S0040-1951(01)00240-2.

Golynsky, A., et al. (2001), ADMAP—Magnetic anomaly map of the Antarctic, vol. 10, scale 1:10,000,000, Br. Antarct. Surv., Cambridge, U. K.

Hemant, K., and S. Maus (2005), Geological modeling of the new CHAMP magnetic anomaly maps using a geographical information system technique, *J. Geophys. Res.*, *110*, B12103, doi:10.1029/2005JB003837.

Hildenbrand, T. G., B. Berger, R. C. Jachens, and S. Ludington (2000), Regional crustal structures and their relationship to the distribution of ore deposits in the western United States, based on magnetic and gravity data, *Econ. Geol.*, *95*, 1583–1603.

Hinze, W. J. (1985), *The Utility of Regional Gravity and Magnetic Anomaly Maps*, Soc. of Explor. Geophys., Tulsa, Okla.

Korhonen, J., et al. (2007), Magnetic anomaly map of the world, scale 1:50,000,000, 1st ed., Geol. Surv. of Finland, Helsinki.

Langel, R. A., and W. J. Hinze (1998), *The Magnetic Field of the Earth's Lithosphere: The Satellite Perspective*, Cambridge Univ. Press, Cambridge, U. K.

Maus, S. (2008), The geomagnetic power spectrum, *Geophys. J. Int.*, *174*, 135–142, doi:10.1111/j.1365-246X.2008.03820.x.

Maus, S., et al. (2005), The 10th-generation International Geomagnetic Reference Field, *Geophys. J. Int.*, *161*, 561–565, doi:10.1111/j.1365-246X.2005.02641.x.

Maus, S., H. Lühr, M. Rother, K. Hemant, G. Balasis, P. Ritter, and C. Stolle (2007a), Fifth-generation lithospheric magnetic field model from CHAMP satellite measurements, *Geochem. Geophys. Geosyst.*, *8*, Q05013, doi:10.1029/2006GC001521.

Maus, S., T. Sazonova, K. Hemant, J. D. Fairhead, and D. Ravat (2007b), National Geophysical Data Center candidate for the World Digital Magnetic Anomaly Map, *Geochem. Geophys. Geosyst.*, *8*, Q06017, doi:10.1029/2007GC001643.

Maus, S., F. Yin, H. Lühr, C. Manoj, M. Rother, J. Rauberg, I. Michaelis, C. Stolle, and R. D. Müller (2008), Resolution of direction of oceanic magnetic lineations by the sixth-generation lithospheric magnetic field model from CHAMP satellite magnetic measurements, *Geochem. Geophys. Geosyst.*, *9*, Q07021, doi:10.1029/2008GC001949.

Menville, M., and J. Paris (2007), Geomagnetic indices in solar-terrestrial physics and space weather, in *Space Weather: Research Towards Applications in Europe*, *Astrophys. Space Sci. Libr.*, vol. 344, pp. 277–288, Springer, Berlin.

Milligan, P. R., and R. Franklin (2004), Magnetic anomaly map of Australia, 4th ed., scale 1:5,000,000, Geosci. Aust., Canberra, A. C. T.

Milligan, P. R., P. Petkovic, and B. J. Drummond (2003), Potential-field datasets for the Australian region: Their significance in mapping basement architecture, *Spec. Pap. Geol. Soc. Am.*, *372*, 129–139.

Müller, R. D., M. Sdrolias, C. Gaina, and W. R. Roest (2008), Age, spreading rates, and spreading asymmetry of the world's ocean crust, *Geochem. Geophys. Geosyst.*, *9*, Q04006, doi:10.1029/2007GC001743.

Nakanishi, M., K. Tamaki, and K. Kobayashi (1992), A new Mesozoic isochron chart of the northwestern Pacific Ocean: Paleomagnetic and tectonic implications, *Geophys. Res. Lett.*, *19*, 693–696, doi:10.1029/92GL00022.

Purucker, M., and K. Whaler (2007), Crustal magnetism, in *Treatise on Geophysics*, vol. 5, *Geomagnetism*, edited by M. Kono, chap. 6, pp. 195–237, Elsevier, Amsterdam.

Roest, W. R., J. Verhoef, and R. Macnab (1995), Magnetic anomalies and tectonic elements of northeast Eurasia, *GSC Open File, 2574*, Geol. Surv. of Can., Dartmouth, N. S.

Sabaka, T. J., N. Olsen, and M. E. Purucker (2004), Extending comprehensive models of the Earth's magnetic field with Ørsted and CHAMP data, *Geophys. J. Int.*, *159*, 521–547, doi:10.1111/j.1365-246X.2004.02421.x.

Saltus, R. W., and T. L. Hudson (2007), Regional magnetic anomalies, crustal strength, and the location of the Northern Cordilleran fold-and-thrust belt, *Geology*, *35*, 567–570.

Shaw, R. D., P. Wellman, P. Gunn, A. J. Whitaker, C. Tarlowski, and M. Morse (1996), Guide to using the Australian Crustal Elements Map, *Aust. Geol. Surv. Organ. Rec., 1996/30*, Geosci. Aust., Canberra, A. C. T.

Somerton, I., S. Campbell, and M. Stewart (2009), Insights into regional structural geology using gravity and magnetic data, *First Break*, *27*, 101–105.

Tontini, F. C., P. Stefanelli, I. Giori, O. Faggioni, and C. Carmisciano (2004), The revised aeromagnetic anomaly map of Italy, *Ann. Geophys.*, *47*, 1547–1555.

Vine, F. J. (1966), Spreading of the ocean floor: New evidence, *Science*, *154*, 1405–1415.

Vine, F. J., and D. H. Matthews (1963), Magnetic anomalies over oceanic ridges, *Nature*, *199*, 947–949.

Whittaker, J. M., R. D. Müller, G. Leitchenkov, H. Stagg, M. Sdrolias, C. Gaina, and A. Goncharov (2007), Major Australian-Antarctic plate reorganization at Hawaiian-Emperor bend time, *Science*, *318*, 83–86, doi:10.1126/science.1143769.